Title
Control of Outer Radial Glial Stem Cell Mitosis in the Human Brain

Journal
Cell Reports, 8(3)

ISSN
2639-1856

Authors
Ostrem, Bridget EL
Lui, Jan H
Gertz, Caitlyn C
et al.

Publication Date
2014-08-01

DOI
10.1016/j.celrep.2014.06.058

Peer reviewed

OPEN ACCESS
CellPress

Cell Reports
Report

Control of Outer Radial Glial Stem Cell Mitosis in the Human Brain

Bridget E.L. Ostrem,[1,2,3] Jan H. Lui,[1,2] Caitlyn C. Gertz,[1,2,3] and Arnold R. Kriegstein[1,2,*]
[1]Department of Neurology, University of California, San Francisco, 35 Medical Center Way, San Francisco, CA 94143, USA
[2]Eli and Edythe Broad Center of Regeneration Medicine and Stem Cell Research, University of California, San Francisco, 35 Medical Center Way, San Francisco, CA 94143, USA
[3]Neuroscience Graduate Program, University of California, San Francisco, 1550 4th Street, San Francisco, CA 94158, USA
*Correspondence: kriegsteina@stemcell.ucsf.edu
http://dx.doi.org/10.1016/j.celrep.2014.06.058

SUMMARY

Evolutionary expansion of the human neocortex is partially attributed to a relative abundance of neural stem cells in the fetal brain called outer radial glia (oRG). oRG cells display a characteristic division mode, mitotic somal translocation (MST), in which the soma rapidly translocates toward the cortical plate immediately prior to cytokinesis. MST may be essential for progenitor zone expansion, but the mechanism of MST is unknown, hindering exploration of its function in development and disease. Here, we show that MST requires activation of the Rho effector ROCK and nonmuscle myosin II, but not intact microtubules, centrosomal translocation into the leading process, or calcium influx. MST is independent of mitosis and distinct from interkinetic nuclear migration and saltatory migration. Our findings suggest that disrupted MST may underlie neurodevelopmental diseases affecting the Rho-ROCK-myosin pathway and provide a foundation for future exploration of the role of MST in neocortical development, evolution, and disease.

INTRODUCTION

The human neocortex is characterized by a marked increase in size and neuronal number as compared to other mammals. Neural stem cells called outer radial glia (oRG), present in large numbers during human, but not rodent, brain development, are thought to underlie this expansion (Hansen et al., 2010; Lui et al., 2011). oRG cells are derived from ventricular radial glia (vRG), the primary neural stem cells present in all mammals (LaMonica et al., 2013; Malatesta et al., 2000; Miyata et al., 2001; Noctor et al., 2001; Shitamukai et al., 2011; Wang et al., 2011). Both progenitor cell types display basal processes oriented toward the cortical plate, along which newborn neurons migrate (Hansen et al., 2010; Misson et al., 1991; Rakic, 1971, 1972). However, oRG cells reside primarily within the outer subventricular zone (oSVZ), closer to the cortical plate than vRG cells, and lack the apical ventricular contact characteristic of vRG cells (Chenn et al., 1998; Hansen et al., 2010). While vRG cell behavior, mitosis, and lineage have been extensively studied (Bentivoglio and Mazzarello, 1999; Hartfuss et al., 2001; Noctor et al., 2001, 2004, 2008; Qian et al., 1998; Taverna and Huttner, 2010), much less is known about regulation of oRG cell proliferation and the unique mitotic behavior of these cells (Betizeau et al., 2013; Gertz et al., 2014; Hansen et al., 2010; LaMonica et al., 2013; Pilz et al., 2013).

oRG cell cytokinesis is immediately preceded by a rapid translocation of the soma along the basal fiber toward the cortical plate, a process termed mitotic somal translocation (MST) (Hansen et al., 2010). Due to the relative abundance of oRG cells in humans, it has been hypothesized that genetic mutations causing significant brain malformations in humans, but minimal phenotypes in mouse models, may affect oRG cell-specific behaviors such as MST (LaMonica et al., 2012). However, the molecular motors driving MST have not been identified, hindering exploration of the function of MST in human brain development and its possible role in disease. MST is reminiscent of interkinetic nuclear migration (INM) of neuroepithelial and vRG cells, in which nuclei of cycling cells migrate back and forth along the basal fiber between the apical and basal boundaries of the ventricular zone in concert with the cell cycle. INM is controlled by the centrosome, the microtubule motors kinesin and dynein, and associated proteins, with actomyosin motors playing an accessory role (Taverna and Huttner, 2010). As oRG cells are derived from vRG cells and display analogous nuclear movements, it has been hypothesized that MST requires similar molecular motors as INM (LaMonica et al., 2012).

We find that MST requires activation of the Rho effector ROCK and nonmuscle myosin II (NMII), but not intact microtubules, centrosomal advancement into the leading process, or calcium influx. Conversely, oRG cell mitosis requires intact microtubules, but not NMII activation, demonstrating that MST and mitosis are mutually dissociable. We examine the expression profiles of genes implicated in the Rho-ROCK-myosin pathway that cause large developmental brain malformations when mutated in humans, but not in mice. Interestingly, several disease genes thought to primarily affect neuronal migration display expression profiles similar to known radial glial genes, consistent with expression in oRG cells. This observation suggests that defects in oRG behaviors such as MST may partially underlie cortical malformations currently attributed to defective neuronal

migration. Together, these results increase our understanding of the cellular and molecular basis for human cortical evolution and have important implications for studying disease mechanisms that cannot be effectively modeled in mice.

RESULTS

MST is thought to contribute to radial expansion of the oSVZ during human brain development (Lui et al., 2011). Supportive of this idea, we imaged oRG cell divisions in human fetal cortical slices at the border of the upper oSVZ and intermediate zone (IZ) during peak neurogenesis and oSVZ growth (gestational weeks 15–20). We observed many divisions in which oRG cells translocated out of the oSVZ and into the IZ, thereby increasing oSVZ size (Movie S1). We found that MST trajectory in the human oSVZ was overwhelmingly toward the cortical plate (Figure 1A). Furthermore, MST frequency and translocation distances were greater in humans as compared to ferrets and mice, species displaying proportionally smaller oSVZ sizes (Figures 1B–1D). These observations are suggestive of a role for MST in human oSVZ expansion. However, in-depth exploration of the function of MST in development and disease first requires an understanding of the underlying molecular mechanisms, which have remained elusive.

We initially hypothesized that MST depends on the same molecular machinery as INM. To determine the relative contributions of microtubule motors and actomyosin to MST, we applied inhibitors of microtubule polymerization and NMII (the most well-characterized myosin in brain development; Tullio et al., 2001; Vallee et al., 2009) to human fetal cortical slice cultures. We performed time-lapse imaging of oRG cell behaviors and quantified translocation (MST) and division frequency in each slice before and after addition of inhibitors or DMSO (control) (Figures 1E–1I and S1). Treatment of slices with a high concentration (100 μM) of blebbistatin, a selective NMII inhibitor, nearly abolished both translocations and divisions (data not shown). However, treatment with a low concentration (5 μM) of blebbistatin caused a significantly greater reduction in translocations than in divisions, suggesting that NMII plays a relatively larger role in MST than in mitosis. Conversely, treatment with the microtubule depolymerizing reagent nocodazole (1 μM) reduced divisions significantly more than translocations. Additionally, nocodazole, but not DMSO or blebbistatin, decreased the proportion of translocations that ended in division. We found that oRG cells express two isoforms of NMII, NMIIa and NMIIb (Figures 1J, 1K, and S1), which have both been shown to play essential roles in neuronal migration (Vicente-Manzanares et al., 2009). These results demonstrate that MST and mitosis are mutually dissociable in oRG cells. MST requires NMII activation, but not intact microtubules, and thus, not microtubule motors. Conversely, mitosis is relatively more dependent on intact microtubules than on NMII activation. We asked whether inhibition of MST directly affects daughter cell fate. Blebbistatin treatment of human fetal cortical slices did not alter the ratio of TBR2+ to SOX2+ cells in the oSVZ as compared to DMSO ($p = 0.38$, unpaired Student's t test), suggesting that MST does not control cell fate. Inhibition of MST may lead to cell crowding or have other indirect effects that could influence cell fate on a longer timescale than we could analyze using our slice culture system.

To control for non-cell-autonomous effects and to enable examination of subcellular mechanisms, we used dissociated neural progenitor cell cultures. Blocks of gestational week 15–20 (GW15–20) dorsal neocortical tissue spanning the ventricle to the cortical plate were dissociated by papain treatment and trituration. We previously observed that oRG-like cells undergo MST in dissociated fetal human cortical cultures (LaMonica et al., 2013). To confirm oRG identity of oRG-like cells, we performed fate staining on daughter cells after MST division (Figures 2A–2C and S2). Similar to oRG cells in slice culture (Hansen et al., 2010), daughters of MST divisions in dissociated culture expressed SOX2 (65 out of 65) and PAX6 (17 out of 17), usually expressed nestin (18 out of 24), rarely expressed TBR2 (2 out of 34), and never expressed βIII-tubulin (0 out of 20). As in slice culture, we observed expression of both NMIIa (14 out of 14 cells) and NMIIb (ten out of ten cells) in dissociated oRG cell daughters (Figures 2I and 2J). We concluded, based on morphology, behavior, and marker expression, that cells undergoing MST in dissociated culture are oRG cells, validating the use of dissociated cultures to study oRG cell behaviors.

We quantified translocation (MST) and division frequency in dissociated culture after motor protein inhibition. Similar to results in slice culture, blebbistatin treatment reduced translocations significantly more than divisions, while nocodazole treatment reduced divisions without significantly affecting translocations (Figures 2D–2H and Movie S2). Upon drug washout, blebbistatin-treated cultures showed an increase in translocations, while nocodazole-treated cells that had remained rounded up after MST underwent cytokinesis, suggesting that the effects of inhibitors were reversible and not due to cell death (Movie S3; Figure S2). Furthermore, inhibitor-treated cultures did not display increased staining for cleaved caspase-3, confirming that the effects of inhibitor treatment could not be attributed to apoptosis (Figure S2). Thus, results in dissociated culture confirm observations in slice culture that MST and mitosis are mutually dissociable in oRG cells. Intact microtubules are required for oRG cell mitosis, but not for MST, while NMII activation is required for oRG cell MST and is relatively less important for mitosis.

Though microtubule polymerization is not required for oRG cell MST in humans, nocodazole treatment significantly increased MST distance in both slice culture and dissociated cells (Figure 3A). Based on previous observations in rodent (Wang et al., 2011), we hypothesized that the centrosome migrates into the basal fiber prior to translocation, remains connected to the nucleus via a microtubule cage, and ultimately determines the location of translocation cessation and cytokinesis (Tsai et al., 2007). Nocodazole treatment would disrupt nucleus-centrosome coupling, eliminating the "stop" signal for translocation. To determine whether the centrosome precedes the nucleus into the basal process, we performed time-lapse imaging of centrosome behavior in dissociated human oRG cells after transfection with a construct encoding the centrosomal protein Centrin-2 (*Cetn2*) fused to the fluorescent reporter dsred (Figure S2) (Tanaka et al., 2004). While centrosome location was variable during interphase, centrosomes consistently returned to the soma prior to MST and remained adjacent to the nucleus throughout translocation (Figures 3B and 3D; Movie S4). In

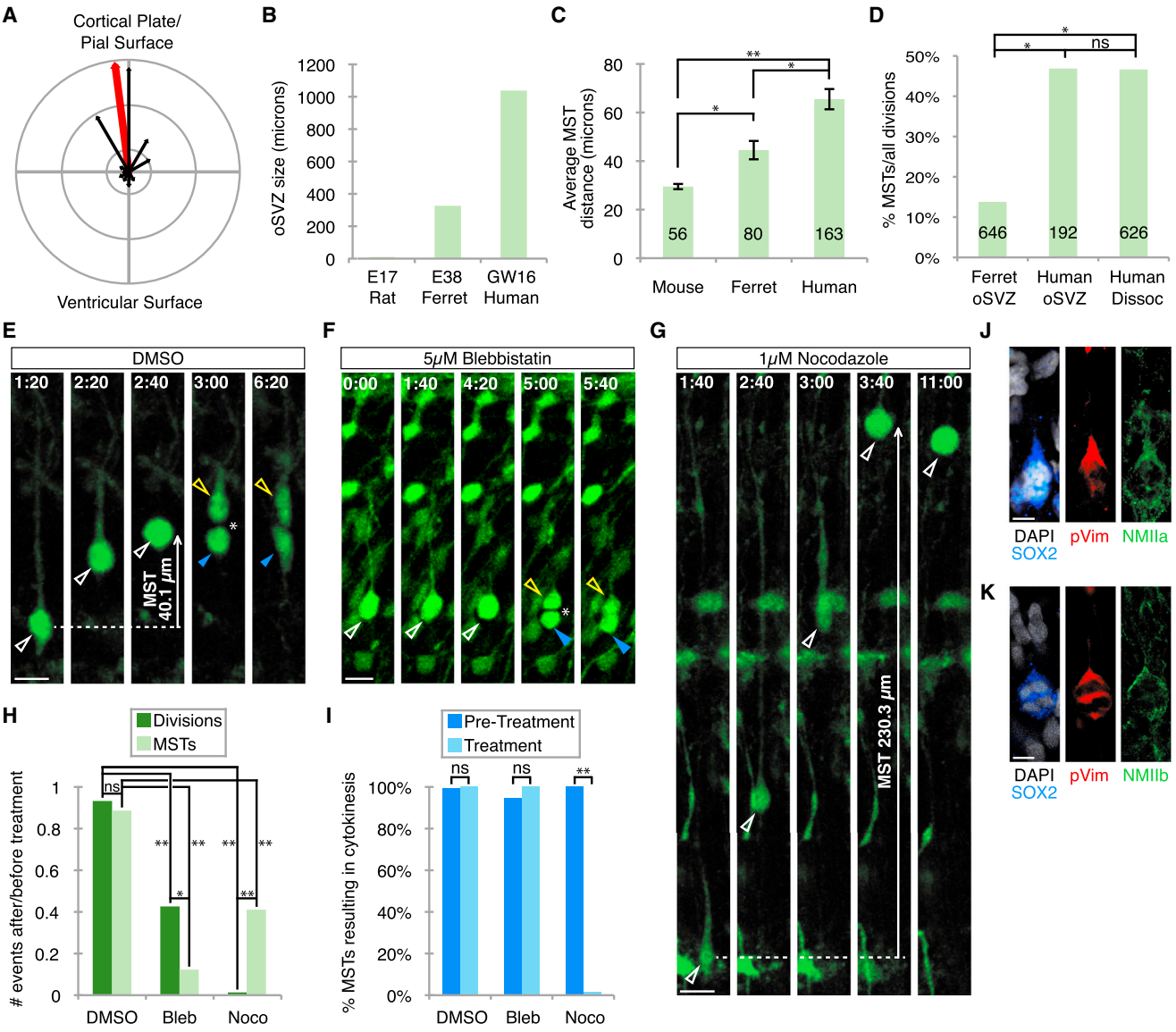

Figure 1. oRG Cell MST Requires Myosin II Activation, but Not Intact Microtubules

(A) Vector plot of MST trajectory angles in human cortical slices (n = 62 MSTs). Angles grouped in 30° increments; lengths of black arrows represent proportion of MSTs of a given angle, and the red arrow depicts net MST trajectory (vector sum).

(B and C) oSVZ sizes and average MST distance in species of analogous gestational ages. (B) Rat and ferret oSVZ measurements are from studies by Martínez-Cerdeño and coworkers (Martínez-Cerdeño et al., 2012). (C) Mouse measurements were reanalyzed from Wang et al. (Wang et al., 2011) to only include translocation distances of ≥20 μm, the definition of MST used in our study. At least three slices from three different tissue samples were summed for ferret and human measurements, and sample sizes are indicated on each column. Error bars, SEM. *p < 0.01. **p < 0.001, unpaired Student's t test.

(D) Proportion of mitoses preceded by MST in the oSVZ of ferret and human fetal cortical slices and in dissociated human fetal cortical cultures. Total number of divisions analyzed are indicated on each column; n ≥ 3 slices from three different tissue samples for ferret and human oSVZ; n = 3 wells for human dissociated cultures. *p < 0.0001, χ^2 test.

(E–G) Time-lapse stills of oRG cell behaviors in GW20.5 human fetal cortical slices labeled with Adeno-GFP. Time is in hours:minutes. Scale bars, 15 μm. (E) In a DMSO (control)-treated slice, the oRG cell (open white arrowhead) undergoes MST and cytokinesis (asterisk) to produce an apical daughter (closed blue arrowhead) and a basal daughter that retains oRG cell morphology (open yellow arrowhead). (F) In a slice treated with the myosin II inhibitor blebbistatin, the oRG cell (open white arrowhead) divides (asterisk) without MST to produce an apical daughter (closed blue arrowhead) and a basal daughter that retains oRG cell morphology (open yellow arrowhead). (G) In a slice treated with the microtubule depolymerizing agent nocodazole, the oRG cell (open white arrowhead) undergoes MST, fails to divide, and remains rounded up at the end of imaging.

(H) Quantification of ratio of divisions and translocations (MSTs) after/before treatment for control (DMSO, 0.5%), blebbistatin (Bleb, 5 μM), and nocodazole (Noco, 1 μM). *p < 0.01, **p < 0.0001, Fisher exact test.

(I) Quantification of % MSTs resulting in cytokinesis. **p < 0.0001, Fisher exact test.

(J and K) oRG cells in GW17.5 human fetal oSVZ express SOX2, the mitotic marker phospho-vimentin (pVIM), NMIIa (J), and NMIIb (K). Scale bars, 5 μm.

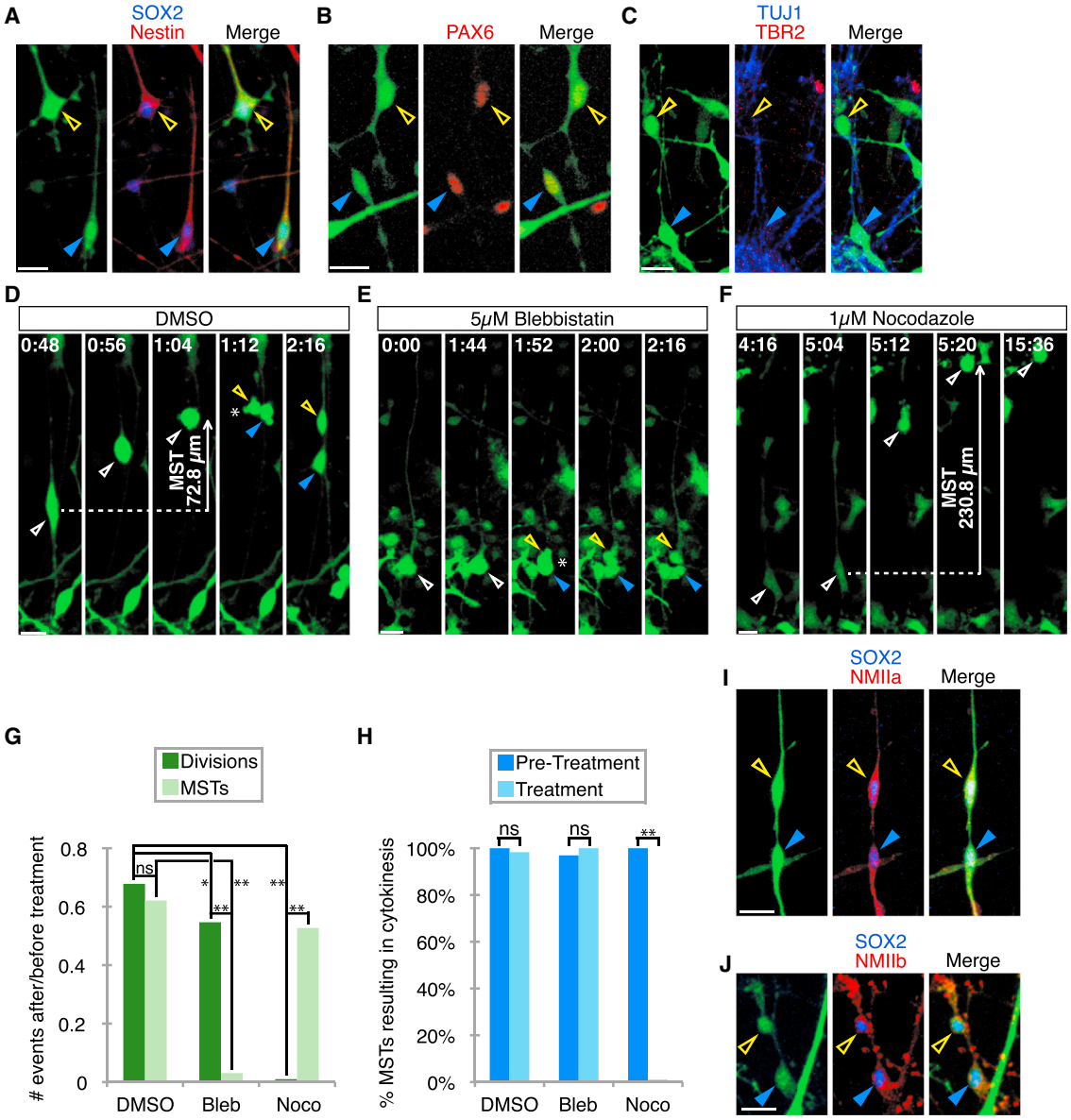

Figure 2. Dissociated Human Cortical Progenitor Cells Express oRG Cell Markers and Require Myosin II for MST

(A–C) Fate staining of daughters (open yellow and solid blue arrowheads) of MST divisions in GW16.5 dissociated fetal human cortical progenitor cell cultures. Scale bars, 20 μm. (A) Both cells express SOX2 and nestin. (B) Both cells express PAX6. (C) Neither cell expresses TUJ1 or TBR2.

(D–F) Time-lapse stills of oRG cells (open white arrowheads) in GW15.5–18.5 dissociated cultures labeled with Adeno-GFP. Time is in hours:minutes. Scale bars, 20 μm. (D) oRG cell in DMSO (control)-treated culture undergoes MST and divides (asterisk) to produce an "apical" daughter (closed blue arrowhead) and a "basal" daughter that retains oRG cell morphology (open yellow arrowhead). (E) Cell with oRG morphology in blebbistatin-treated culture divides (asterisk) without MST to produce an "apical" daughter (closed blue arrowhead) and a "basal" daughter that retains oRG cell morphology (open yellow arrowhead). (F) oRG cell in nocodazole-treated culture undergoes MST, fails to divide, and remains rounded up at the end of imaging.

(G) Quantification of ratio of divisions and translocations (MSTs) after/before treatment for control (DMSO, 0.5%), blebbistatin (Bleb, 5 μM), and nocodazole (Noco, 1 μM). *$p < 0.05$, **$p < 0.0001$, Pearson's chi-square test or Fisher exact test (depending on sample size).

(H) Quantification of % MSTs resulting in cytokinesis. **$p < 0.0001$, Fisher exact test.

(I and J) Fate staining of daughters of MST divisions in GW16 dissociated fetal human cortical progenitor cell cultures. Daughter cells (indicated with open yellow and closed blue arrowheads) express the oRG cell marker SOX2 and the myosin isoforms NMIIa (I) and NMIIb (J). Scale bars, 20 μm.

contrast, during saltatory migration of other cells in dissociated culture, the centrosome often preceded the nucleus into the leading process prior to a migratory step (Figures 3C and 3D; Movie S4). Interestingly, somal translocation distances were much greater during MST than during saltatory migration steps, suggesting that an increased translocation distance may limit the

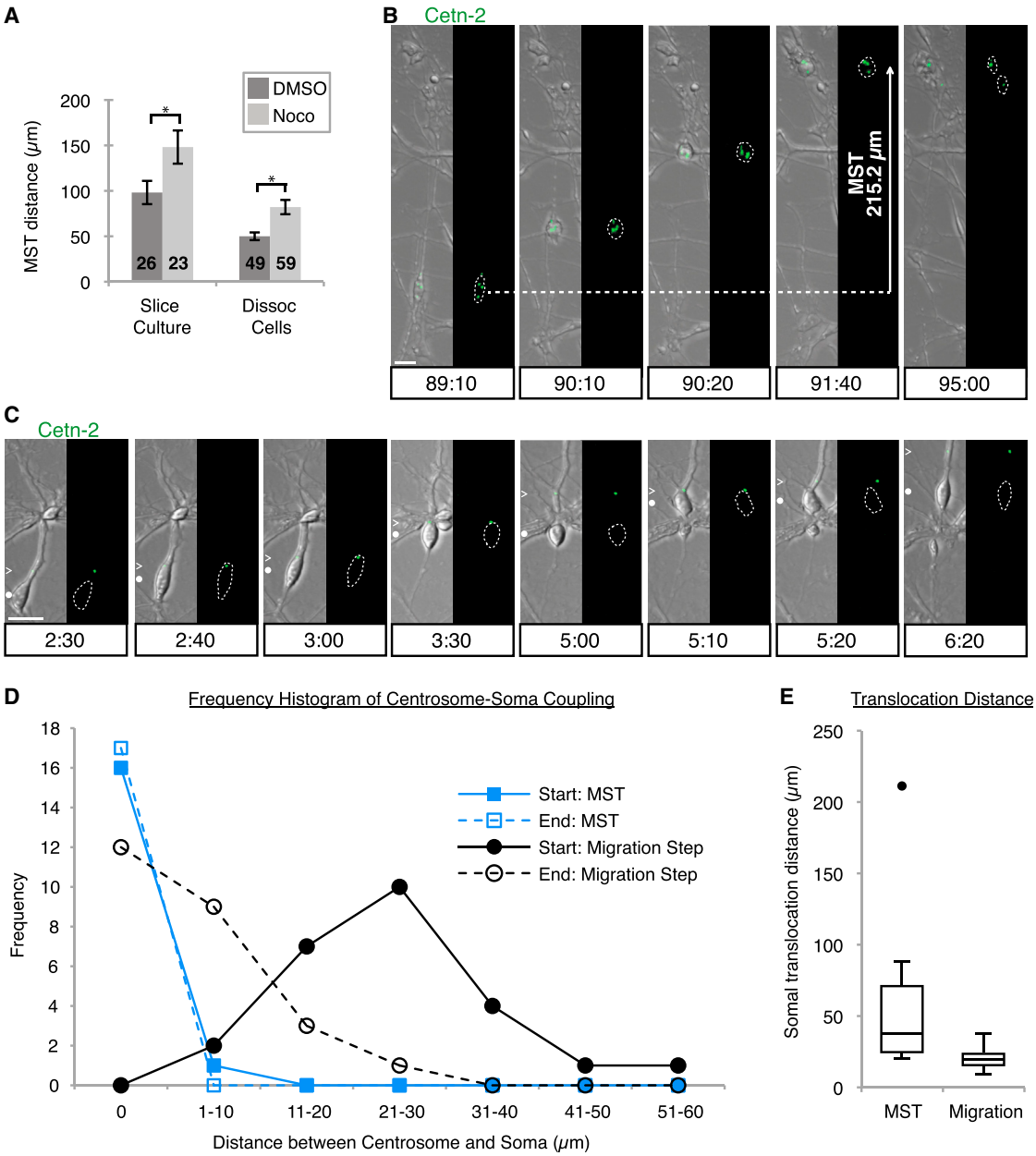

Figure 3. Role of Microtubules and the Centrosome in MST

(A) Quantification of MST distances after treatment with DMSO (control, 0.5%) or nocodazole (Noco, 1 μM). *$p < 0.05$, unpaired Student's t test. Error bars are SEM; sample size is indicated on each bar.

(B and C) Time-lapse stills of oRG cell and centrosome behaviors in GW18.5 dissociated culture transfected with dsred-Cent2 to label centrosomes. Cent2 (*Cetn2*) is false-colored in green. Each time point shows transmitted light and cent2 merge on the left and cent2 on the right, with a dashed white line depicting the outline of the soma. Time is in hours:minutes. Scale bars, 20 μm. (B) oRG cell undergoes MST with centrosomes adjacent to the nucleus. (C) Centrosome behavior in cell undergoing saltatory migration. The location of the centrosome (white arrowhead) and the center of the soma (white circle) in the axis parallel to the direction of migration are shown on the left side of the transmitted light images.

(D) Frequency histogram showing distances between the edge of the soma and the center of the centrosome furthest from the soma (C-S distance). The average C-S distance is 0.37 μm at the start, and 0 μm (centrosomes within the soma) at the end of MST, whereas the C-S distance during a migratory step averages 23.8 μm at the start, and 4.2 μm at the end.

(E) Boxplots depicting somal translocation distances of cells analyzed in (D) during MST (left) and migratory steps (right); n = 17 for MSTs, n = 21 for migratory steps.

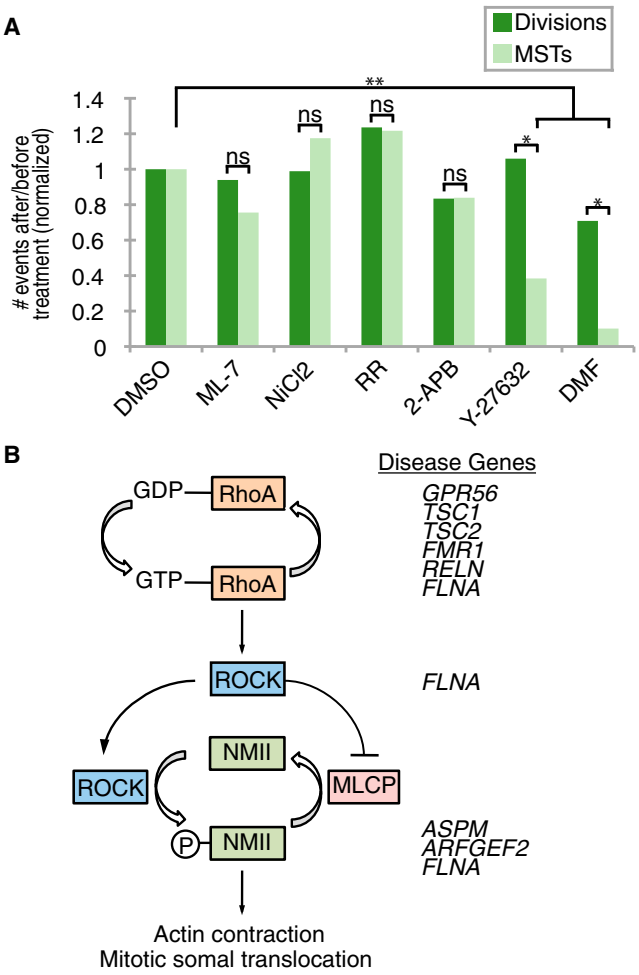

Figure 4. MST Is Dependent on ROCK Signaling, but Not Calcium Influx

(A) Quantification of ratio of divisions and translocations (MSTs) after/before treatment with DMSO; myosin light chain kinase inhibitor ML-7; calcium channel blockers $NiCl_2$, ruthenium red (RR), and 2-APB; or ROCKi inhibitors Y-27632 and dimethylfasudil (DMF). *$p < 0.05$, **$p < 0.0001$, Fisher exact test. Unless otherwise indicated, inhibitor treatments were not significantly different from DMSO.

(B) Proposed molecular pathway controlling MST. Genes associated with human cortical malformations that have previously been demonstrated to regulate specific pathway proteins are shown next to those proteins. MLCP, myosin phosphatase.

role of the centrosome during MST (Figure 3E). We concluded that MST does not require centrosomal advancement into the leading process prior to nuclear translocation. Instead, microtubule polymerization may directly regulate actomyosin contractility (Schaar and McConnell, 2005).

Our results thus far suggested that MST does not require intact microtubules or centrosomal translocation into the basal process, but that MST is dependent on NMII activation. To verify that the effects of blebbistatin on MST were specifically due to NMII inhibition, we tested whether inhibition of ROCK, an upstream activator of NMII, similarly blocked MSTs (Govek et al., 2011). Treatment of dissociated cultures with the ROCK inhibitor Y-27632 (10μM) mimicked the effects of blebbistatin treatment, greatly reducing translocations without significantly affecting divisions (Figure 4A). While blebbistatin had a small effect on mitosis, ROCK inhibition had no effect, likely due to myosin playing a bigger role in oRG cell cytokinesis than ROCK. Treatment with a second, more potent and selective ROCK inhibitor, dimethylfasudil (1 μM), mimicked blebbistatin and Y-27632 treatment, reducing translocations without significantly affecting divisions (Figure 4A). These results confirm that the effects of blebbistatin on MST are specifically due to NMII inhibition, and suggest that the Rho-ROCK-NMII pathway may control MST, as ROCK is activated by the GTPase RhoA (Heng and Koh, 2010). ROCK- and NMII-dependent actomyosin contraction may occur throughout the soma and basal process, as we often observed shortening and thinning of the primary process during MST in dissociated oRG cells (Figure S2). This observation is consistent with NMII expression throughout oRG cell processes (Figures 2I and 2J).

We asked whether calcium influx, a parallel activator of NMII, is required for MST. We treated human fetal progenitor cultures with ML-7, an inhibitor of myosin light chain kinase (MLCK). MLCK activates NMII and is downstream of Ca^{2+}-calmodulin, but not ROCK. ML-7 (10 μM) had no effect on translocations or divisions (Figure 4A). We further verified these results by subjecting dissociated cultures to treatment with a panel of calcium channel inhibitors, including the nonspecific calcium channel blocker $NiCl_2$ (50 μM), ryanodine receptor blocker ruthenium red (50 μM), and the IP_3-gated calcium channel blocker 2-APB (50 μM). Calcium channel inhibition had no effect on either translocations or divisions (Figure 4A). These results suggest that calcium influx is not responsible for NMII activation leading to MST.

DISCUSSION

We have demonstrated here that MST and mitosis can be uncoupled, and that MST requires ROCK and NMII activation, but not intact microtubules, centrosomal translocation into the leading process, or calcium influx. It is possible that in oRG cells, RhoA-activated ROCK either directly phosphorylates NMII, inhibits myosin phosphatase, or both, leading to actomyosin contraction and MST (Figure 4B). The expression and activity of known cell-cycle regulators support a role for the Rho-ROCK-myosin pathway in MST: RhoA is activated in a cell cycle-dependent manner by CDK1, and RhoA has been demonstrated to participate in the G_2 to M transition (Heng and Koh, 2010). Several evolutionary forces could have led to the unique dependence of MST on actomyosin motors. Nuclear translocation distance may dictate molecular motor dependence. Interkinetic nuclear migration and saltatory migration involve small nuclear translocation steps, limiting the distance between the centrosome and the nucleus. The larger translocation distances of MST could hinder maintenance of tension between the centrosome and a perinuclear microtubule cage, making a centrosome-based mechanism untenable. Actomyosin motors are also approximately 10-fold faster than microtubule motors, and may be better suited to drive the rapid, large-amplitude translocations of MST (Månsson, 2012). Additionally, we observed chromosome condensation and establishment of

a metaphase plate during MST using time-lapse transmitted light microscopy, suggesting that prophase and metaphase occur prior to the completion of MST (Figure 3B; Movie S4). Microtubule depolymerization occurs during prometaphase and may preclude dependence of MST on microtubule motors (Rusan et al., 2002).

A recent study suggested a broader diversity of progenitor cell types and behaviors within the macaque oSVZ than we observed in humans, including a larger proportion of apically directed MSTs (Betizeau et al., 2013). While the definition of oRG cells used by Betizeau and colleagues is more ambiguous than ours, it is clear that at least a subset of oSVZ progenitor cells display basally directed MST that shifts the border of the oSVZ toward the cortical plate, appearing to expand oSVZ size by moving neural stem cells further away from the ventricle. Thus, while we observed that MST does not directly control cell fate, MST may accelerate fetal brain development by delivering oRG daughters, including intermediate progenitor cells and their neuronal progeny, closer to their destinations in the cortical plate (Hansen et al., 2010; Wang et al., 2011). Apically directed MST, along with other oSVZ progenitor cell behaviors not described in our study, may also function to reduce cell crowding. It is possible that discrepancies in oRG behaviors observed in macaques and humans reflect species-specific differences in MST function or a labeling bias in one or both studies. Alternatively, Betizeau and colleagues may have interpreted apically directed progenitor cell migration followed by division as MST due to a lower sampling frequency (one frame per 1–1.5 hr) than ours (one frame per 8–20 min).

We wondered whether MST and other oRG-specific behaviors are affected in human neurodevelopmental disorders. Several genetic mutations that target the Rho-ROCK-myosin pathway lead to cortical malformations in humans that have historically been attributed to defective neuronal migration (Figure 4; Table S1). However, our finding that MST depends on this pathway suggests that MST may also be affected. Indeed, the expression patterns within the fetal human cortex of several cortical malformation candidate genes resemble the expression patterns of known radial glial genes, and hence of oRG cells, more closely than those of immature neuronal genes (Figure S3). oRG cells comprise only a small proportion of neural progenitor cells in mice as compared to humans (Wang et al., 2011), and this difference could help explain why mouse models of cortical malformations such as microcephaly, periventricular heterotopia, and lissencephaly often display relatively mild phenotypes (Table S1). Future studies may reveal that mutations that affect the Rho-ROCK-myosin pathway and have minimal or altered phenotypes when reproduced in mouse models primarily target MST and not neuronal migration in human patients.

EXPERIMENTAL PROCEDURES

Fetal Tissue Collection

Fetal brain tissue was collected from elective pregnancy termination specimens at San Francisco General Hospital, and was transported in ice-chilled artificial cerebrospinal fluid (ACSF) to the laboratory for further processing. Tissues were collected only with previous patient consent and in strict observance of legal and institutional ethical regulations. Research protocols were approved by the Gamete, Embryo, and Stem Cell Research Committee (institutional review board) at University of California, San Francisco. See Supplemental Experimental Procedures for further details.

Slice Culture and Real-Time Imaging

Blocks of tissue from GW15–20 fetal dorsal cortex were imbedded in agarose, and 300 μm vibratome slices were generated and transferred to cortical slice culture medium containing CMV-GFP adenovirus. After labeling, slices were imaged using an inverted Leica TCS SP5 with an on-stage incubator at 15–25 min intervals for up to 6 days. Maximum intensity projections of the collected stacks were compiled and generated into movies, which were analyzed using Imaris. See Supplemental Experimental Procedures for further details.

Dissociated Cortical Progenitor Culture and Real-Time Imaging

Dorsal cortical tissue was subjected to papain-based dissociation, and dissociated cells were plated at a density of 500,000–1,000,000 cells per well in matrigel-coated 12-well cell culture plates. Cultures were maintained in a Dulbecco's modified Eagle's medium-based dissociated culture medium. For cell fate and inhibitor experiments, cells were labeled with CMV-GFP adenovirus. For centrosome imaging experiments, cells were transfected with dsred-Cent2 (*Cetn2*) plasmid (Addgene plasmid 29523). Cultures were transferred to an inverted Leica TCS SP5 with an on-stage incubator and imaged using a ×10 objective at 8 min to 20 min intervals. See Supplemental Experimental Procedures for further details.

Chemical Inhibitors

Stock solutions of inhibitors were as follows: blebbistatin (100 mM in DMSO), nocodazole (2 mM in DMSO), Y-27632 (10 mM in DMSO), dimethylfasudil (10 mM in water), ML-7 (10 mM in DMSO), NiCl2 (1 M in water), ruthenium red (10 mM in DMSO), and 2-aminoethoxydiphenyl borate (2-APB) (Sigma; 10 mM in DMSO). Control treatment was 0.5% DMSO, which was greater than or equal to the final DMSO concentration for each inhibitor. See Supplemental Experimental Procedures for further details.

Immunohistochemistry

See Supplemental Experimental Procedures for a detailed description of methods, which were standard procedures.

Ferret Slice Culture and Real-Time Imaging

Embryonic day 27 (E27) timed-pregnant ferrets were obtained from Marshall BioResources and maintained according to protocols approved by the Institutional Animal Care and Use Committee at the University of California, San Francisco. E39 pregnant dams were deeply anesthetized with ketamine followed by isoflurane administration. Ovariohysterectomy for fetus collection was then performed and embryonic brains, along with meninges, removed in ice-chilled ACSF bubbled with 95% O_2/5% CO_2. The dorsal cortex was dissected away from ventral structures, imbedded in 3% low-melting-point agarose in ACSF, and sectioned using a vibratome to obtain 250–300 μm slices. Slices were transferred to cortical slice culture medium and treated as described for human slices, including labeling with Adeno-GFP and imaging using an inverted Leica TCS SP5 microscope. Maximum-intensity projections of the collected stacks were compiled and generated into movies, which were analyzed using Imaris.

Measurement of MST Distances, MST Trajectory, and oSVZ Size

MST was defined as a translocation of greater than or equal to 20 μm (approximately one cell diameter) of the soma along the basal process (slice culture) or the primary process (dissociated culture), with a velocity of greater than or equal to 20 μm/hr, coinciding with cell rounding, and ending either in immediate cytokinesis or in a prolonged, rounded state. Angle with respect to the ventricular surface was measured, and trajectories were grouped in increments of 30°. A vector sum was computed to determine the overall trajectory of all MSTs. See Supplemental Experimental Procedures for further details.

Microarray Profiling

To examine the expression across brain regions of genes associated with human neurodevelopmental diseases, we used the BrainSpan laser

microdissection and microarray profiling data set made available by the Allen Institute (BrainSpan, 2011). The data set was generated from four brains of ages GW17, 18, 23, and 23.5, which were cryosectioned, microdissected, and subjected to mRNA profiling by hybridization to custom Agilent microarrays. See Supplemental Experimental Procedures for further details.

Statistics

All quantifications were performed blind, and p values < 0.05 were considered statistically significant. See Supplemental Experimental Procedures for a detailed description of statistical methods.

SUPPLEMENTAL INFORMATION

Supplemental Information includes Supplemental Experimental Procedures, three figures, one table, and four movies and can be found with this article online at http://dx.doi.org/10.1016/j.celrep.2014.06.058.

AUTHOR CONTRIBUTIONS

B.E.L.O. and A.R.K. designed the experiments; B.E.L.O. and J.H.L. carried out all experiments except those with ferret tissue and performed quantifications and analyses; C.C.G. performed ferret experiments; B.E.L.O. and A.R.K. wrote the initial manuscript; and all authors edited and approved the final manuscript.

ACKNOWLEDGMENTS

We thank A. Alvarez-Buylla, J. Chan, and members of the Kriegstein laboratory for thoughtful discussions and critical reading of the manuscript. We thank W. Walantus, Y.Y. Wang, and S. Wang for technical support. We thank Dr. J. Gleeson for use of the dsred-Cent2 (*Cetn2*) plasmid. We thank the staff at the San Francisco General Hospital for providing access to donated fetal tissue. The research was made possible by a grant from the California Institute for Regenerative Medicine (grant number TG2-01153). Additionally, this work was supported by Bernard Osher and by award number R01NS075998 from the NINDS. The contents of this publication are solely the responsibility of the authors and do not necessarily represent the official views of CIRM or any other agency of the State of California or of the NINDS or the NIH.

Received: January 13, 2014
Revised: May 17, 2014
Accepted: June 26, 2014
Published: July 31, 2014

REFERENCES

Bentivoglio, M., and Mazzarello, P. (1999). The history of radial glia. Brain Res. Bull. *49*, 305–315.

Betizeau, M., Cortay, V., Patti, D., Pfister, S., Gautier, E., Bellemin-Ménard, A., Afanassieff, M., Huissoud, C., Douglas, R.J., Kennedy, H., and Dehay, C. (2013). Precursor diversity and complexity of lineage relationships in the outer subventricular zone of the primate. Neuron *80*, 442–457.

BrainSpan. (2011). Atlas of the Developing Human Brain. Funded by ARRA awards 1RC2MH089921-01, 1RC2MH090047-01, and 1RC2MH089929-01. http://developinghumanbrain.org.

Chenn, A., Zhang, Y.A., Chang, B.T., and McConnell, S.K. (1998). Intrinsic polarity of mammalian neuroepithelial cells. Mol. Cell. Neurosci. *11*, 183–193.

Gertz, C.C., Lui, J.H., LaMonica, B.E., Wang, X., and Kriegstein, A.R. (2014). Diverse behaviors of outer radial glia in developing ferret and human cortex. J. Neurosci. *34*, 2559–2570.

Govek, E.E., Hatten, M.E., and Van Aelst, L. (2011). The role of Rho GTPase proteins in CNS neuronal migration. Dev. Neurobiol. *71*, 528–553.

Hansen, D.V., Lui, J.H., Parker, P.R., and Kriegstein, A.R. (2010). Neurogenic radial glia in the outer subventricular zone of human neocortex. Nature *464*, 554–561.

Hartfuss, E., Galli, R., Heins, N., and Götz, M. (2001). Characterization of CNS precursor subtypes and radial glia. Dev. Biol. *229*, 15–30.

Heng, Y.W., and Koh, C.G. (2010). Actin cytoskeleton dynamics and the cell division cycle. Int. J. Biochem. Cell Biol. *42*, 1622–1633.

LaMonica, B.E., Lui, J.H., Wang, X., and Kriegstein, A.R. (2012). OSVZ progenitors in the human cortex: an updated perspective on neurodevelopmental disease. Curr. Opin. Neurobiol. *22*, 747–753.

LaMonica, B.E., Lui, J.H., Hansen, D.V., and Kriegstein, A.R. (2013). Mitotic spindle orientation predicts outer radial glial cell generation in human neocortex. Nat. Commun. *4*, 1665.

Lui, J.H., Hansen, D.V., and Kriegstein, A.R. (2011). Development and evolution of the human neocortex. Cell *146*, 18–36.

Malatesta, P., Hartfuss, E., and Götz, M. (2000). Isolation of radial glial cells by fluorescent-activated cell sorting reveals a neuronal lineage. Development *127*, 5253–5263.

Månsson, A. (2012). Translational actomyosin research: fundamental insights and applications hand in hand. J. Muscle Res. Cell Motil. *33*, 219–233.

Martínez-Cerdeño, V., Cunningham, C.L., Camacho, J., Antczak, J.L., Prakash, A.N., Cziep, M.E., Walker, A.I., and Noctor, S.C. (2012). Comparative analysis of the subventricular zone in rat, ferret and macaque: evidence for an outer subventricular zone in rodents. PLoS ONE *7*, e30178.

Misson, J.P., Austin, C.P., Takahashi, T., Cepko, C.L., and Caviness, V.S., Jr. (1991). The alignment of migrating neural cells in relation to the murine neopallial radial glial fiber system. Cereb. Cortex *1*, 221–229.

Miyata, T., Kawaguchi, A., Okano, H., and Ogawa, M. (2001). Asymmetric inheritance of radial glial fibers by cortical neurons. Neuron *31*, 727–741.

Noctor, S.C., Flint, A.C., Weissman, T.A., Dammerman, R.S., and Kriegstein, A.R. (2001). Neurons derived from radial glial cells establish radial units in neocortex. Nature *409*, 714–720.

Noctor, S.C., Martínez-Cerdeño, V., Ivic, L., and Kriegstein, A.R. (2004). Cortical neurons arise in symmetric and asymmetric division zones and migrate through specific phases. Nat. Neurosci. *7*, 136–144.

Noctor, S.C., Martínez-Cerdeño, V., and Kriegstein, A.R. (2008). Distinct behaviors of neural stem and progenitor cells underlie cortical neurogenesis. J. Comp. Neurol. *508*, 28–44.

Pilz, G.A., Shitamukai, A., Reillo, I., Pacary, E., Schwausch, J., Stahl, R., Ninkovic, J., Snippert, H.J., Clevers, H., Godinho, L., et al. (2013). Amplification of progenitors in the mammalian telencephalon includes a new radial glial cell type. Nat. Commun. *4*, 2125.

Qian, X., Goderie, S.K., Shen, Q., Stern, J.H., and Temple, S. (1998). Intrinsic programs of patterned cell lineages in isolated vertebrate CNS ventricular zone cells. Development *125*, 3143–3152.

Rakic, P. (1971). Guidance of neurons migrating to the fetal monkey neocortex. Brain Res. *33*, 471–476.

Rakic, P. (1972). Mode of cell migration to the superficial layers of fetal monkey neocortex. J. Comp. Neurol. *145*, 61–83.

Rusan, N.M., Tulu, U.S., Fagerstrom, C., and Wadsworth, P. (2002). Reorganization of the microtubule array in prophase/prometaphase requires cytoplasmic dynein-dependent microtubule transport. J. Cell Biol. *158*, 997–1003.

Schaar, B.T., and McConnell, S.K. (2005). Cytoskeletal coordination during neuronal migration. Proc. Natl. Acad. Sci. USA *102*, 13652–13657.

Shitamukai, A., Konno, D., and Matsuzaki, F. (2011). Oblique radial glial divisions in the developing mouse neocortex induce self-renewing progenitors outside the germinal zone that resemble primate outer subventricular zone progenitors. J. Neurosci. *31*, 3683–3695.

Tanaka, T., Serneo, F.F., Higgins, C., Gambello, M.J., Wynshaw-Boris, A., and Gleeson, J.G. (2004). Lis1 and doublecortin function with dynein to mediate coupling of the nucleus to the centrosome in neuronal migration. J. Cell Biol. *165*, 709–721.

Taverna, E., and Huttner, W.B. (2010). Neural progenitor nuclei IN motion. Neuron *67*, 906–914.

Tsai, J.W., Bremner, K.H., and Vallee, R.B. (2007). Dual subcellular roles for LIS1 and dynein in radial neuronal migration in live brain tissue. Nat. Neurosci. *10*, 970–979.

Tullio, A.N., Bridgman, P.C., Tresser, N.J., Chan, C.C., Conti, M.A., Adelstein, R.S., and Hara, Y. (2001). Structural abnormalities develop in the brain after ablation of the gene encoding nonmuscle myosin II-B heavy chain. J. Comp. Neurol. *433*, 62–74.

Vallee, R.B., Seale, G.E., and Tsai, J.W. (2009). Emerging roles for myosin II and cytoplasmic dynein in migrating neurons and growth cones. Trends Cell Biol. *19*, 347–355.

Vicente-Manzanares, M., Ma, X., Adelstein, R.S., and Horwitz, A.R. (2009). Non-muscle myosin II takes centre stage in cell adhesion and migration. Nat. Rev. Mol. Cell Biol. *10*, 778–790.

Wang, X., Tsai, J.W., LaMonica, B., and Kriegstein, A.R. (2011). A new subtype of progenitor cell in the mouse embryonic neocortex. Nat. Neurosci. *14*, 555–561.